Analog Integrated Circuits and Signal Processing (2025) 123:4
https://doi.org/10.1007/s10470-025-02355-7

Integration of metamaterials for quintuple band-notched ultra-wideband antennas

Sapna Arora[1] · Sharad Sharma[2] · Rohit Anand[3] · Anupma Gupta[4] · Ramesh Kumar[4] · Ahmed Jamal Abdullah Al-Gburi[5]

Received: 22 October 2023 / Revised: 3 February 2025 / Accepted: 10 February 2025 / Published online: 25 February 2025

Abstract

This paper presents an elliptical monopole antenna integrated with metamaterial structures to achieve band-notched characteristics. Five narrowband spectrums are notched to mitigate interference in the ultra-wideband (UWB) spectrum. Satellite communication in the C-band (3.7 to 4.2 GHz) and the wireless local area network (WLAN) band (5.15 to 5.35 GHz) are suppressed by etching dual elliptical split-ring resonators (ESRRs) into the monopole radiator. A 2-via dual-slot electromagnetic band-gap (EBG) structure is designed on the left side of the feed line, which results in the rejection of the INSAT band (4.5 to 4.7 GHz) and the upper WLAN band (5.725 to 5.825 GHz). Additionally, the ITU band (7.95 to 8.55 GHz) is rejected by implementing a step-impedance resonator (SIR) on the right side of the feed line. The proposed antenna achieves a 10 dB impedance bandwidth of 8.5 GHz, covering the frequency range from 2.5 to 11.0 GHz, with miniaturized dimensions of $0.317\lambda \times 0.317\lambda \times 0.007\lambda$. A mathematical model is employed to explain the behavior of the notched frequencies and is validated through the simulated surface current distribution. Across the entire passband, a consistent gain of 3 dB is achieved. The proposed structure is well-suited for UWB communication applications.

Keywords Electromagnetic band gap (EBG) · Elliptical radiator · Metamaterial · Quintuple · Step impedance resonator (SIR) · Ultra-wideband (UWB)

1 Introduction

Ultra-wideband (UWB) technology is widely utilized in various wireless applications due to its high-speed data transmission, cost-effectiveness, low emission power, low power spectral density, and strong resistance to multipath environments. UWB systems have a broad range of applications, including medical imaging, wireless body area networks (WBANs), radar systems, military applications, the Internet of Things (IoT), and other communication domains [1–4]. In UWB systems, achieving an omnidirectional radiation pattern and a wide impedance bandwidth is essential for antenna performance [5, 6]. Monopole antennas with planar structures are considered excellent candidates for UWB systems due to their compact size, ease of integration with planar circuits, cost-effectiveness, and lightweight design.

The frequency band of 3.1 to 10.6 GHz was allocated for commercial applications by the Federal Communications Systems in 2002 [7]. Multiple narrowband systems coexist inside the UWB spectrum, which has the potential to create interference in UWB applications. Some commonly

✉ Ahmed Jamal Abdullah Al-Gburi
ahmedjamal@ieee.org; ahmedjamal@utem.edu.my

1 Panipat Institute of Engineering and Technology, Samalkha, Panipat, India

2 MM(DU), Mullana, Ambala, Haryana, India

3 G.B.Pant DSEU Okhla-1 Campus (Formerly GBPEC), New Delhi, India

4 Department of Electronics and Communication Engineering, Saveetha School of Engineering, Saveetha Institute of Medical and Technical Sciences, Thandalam, Chennai, Tamilnadu 602105, India

5 Fakulti Teknologi dan Kejuruteraan Elektronik dan Komputer (FTKEK), Center for Telecommunication Research & Innovation (CeTRI), Universiti Teknikal Malaysia Melaka (UTeM), Jalan Hang Tuah Jaya, Durian Tunggal, 76100 Melaka, Malaysia

used narrowband systems that operate within the ultra-wideband (UWB) range include WiMAX (IEEE 802.16) in the frequency range of 3.3–3.7 GHz, WLAN (IEEE 802.11) which spans from 5.15–5.35 GHz and 5.725–5.825 GHz, the C band for satellite communications with a downlink frequency of 3.77–4.2 GHz and an uplink frequency of 5.9–6.4 GHz, and the ITU frequency band ranging from 7.95 to 8.55 GHz. This study presents a compact UWB antenna with several filters to reduce interference from narrowband systems, hence improving the performance of UWB systems [8–13].

The UWB design being proposed utilizes U-shaped slots that are etched on a circular patch. This design allows for the creation of four notch bands, resulting in a wide bandwidth that spans from 2.9 to 20 GHz [14]. The creation of a rectangular-shaped slot in the partial ground plane allows for the achievement of this. In addition, a bevelled rectangular monopole antenna is proposed in reference [15]. This antenna has semi-circular slots and L-shaped slots on the patch to selectively attenuate signals in the X-band and WiMAX band. Furthermore, a semi-circular stub is added on the substrate's opposite side and attached to the patch using cylindrical pins in order to attenuate the WiMAX band.

2 Existing literature

However, several designs in the existing literature display certain constraints, including complex geometry, restricted control over notch bandwidth, and excessive coupling between band-notch structures [16–18]. In order to address these problems, antenna designs use Electromagnetic Band Gap (EBG) structures, which belong to a specific category of metamaterials [19–21]. These metamaterials exhibit distinctive characteristics of band gaps and have a high impedance at their resonant frequency [22]. The EBG structure, when placed strategically close to the antenna's feed line, acts as a band-stop filter. Its band gap characteristic can be efficiently utilised to generate notch bands.

Mushroom-type Electromagnetic Band Gap (EBG) structures are utilised in Ultra-Wideband (UWB) monopole designs [16–19] to regulate the breadth of notches and generate targeted notch bands. An example of a monopole UWB antenna, as described in reference [23–27], includes a small two-via EBG structure positioned close to the feed line. This structure is designed to provide a single notch specifically for the upper WLAN band, which operates at frequencies between 5.725 GHz and 5.825 GHz. Dual notches are obtained in an alternative design [24] by utilising inverted pi-notch and spiral-shaped EBG structures. It is important to remark that in the designs stated above, a single Electromagnetic Band Gap (EBG) element is only useful in suppressing one notch [28, 29].

The proposed design incorporates a structure that utilises two via double-slot-type Electromagnetic Band Gap (TVDS-EBG), resulting in the achievement of dual notches. This is owing to the presence of two vias within a single cell. Moreover, there is a lack of study on Ultra-Wideband (UWB) antennas that incorporate a Penta-notch arrangement. The present study introduces an elliptically shaped monopole ultra-wideband (UWB) patch antenna with five notches. The antenna has two elliptical split ring resonators (ESRRs) within the radiation patch, in addition to a compact dual-band electromagnetic bandgap (EBG) structure and a stepped impedance resonator (SIR) located near the feed line. This combination is specifically engineered to produce a band with five distinct notches simultaneously.

The inclusion of elliptical split ring resonators (ESRRs) in the antenna patch is essential for creating two distinct gaps in the C band satellite downlink (3.7–4.2 GHz) and the lower WLAN band (5.15–5.35 GHz). Simultaneously, a compact dual-band Electromagnetic Band Gap (EBG) structure is utilised to create dual notches that cover the INSAT band (4.5–4.7 GHz) and the upper WLAN band (5.725–5.825 GHz). Additionally, a Stepped Impedance Resonator (SIR) positioned near the feed line is employed to suppress the ITU band (7.95–8.55 GHz). Hence, the suggested configuration efficiently eliminates five notch bands within the Ultra-Wideband (UWB) spectrum. In addition, the antenna is used in other frequency ranges, such as S (1.97–2.69 GHz), LTE (450 MHz–3.8 GHz), C (3.4–7.025 GHz), X (7.25–8.44 GHz), and Ku (10.7–14.5 GHz). The antenna's design and numerical simulations are performed using High-Frequency Simulation Software (HFSS). The proposed band notch structure has advantage over the UWB antenna. A band-rejected UWB (Ultra-Wideband) antenna with a band-notch feature is designed to operate over a wide frequency range while selectively suppressing specific frequency bands. This capability makes it useful in various applications, including:

- Reduce Interference-Band notch characteristics of proposed antenna mitigates the interference from different narrowband wireless communication links like WiMAX (3.3–3.7 GHz) and WLAN (5.15–5.85 GHz), and provides reliable communication.
- Cognitive Radio—It supports cognitive radio systems and avoids licensed frequency bands and uses the spectrum resourcefully.
- Short-Range Radar Systems—It avoids collision in ground-penetrating radar (GPR) and gives through-wall imaging benefit.
- Wireless Body Area Networks (WBANs)—It ensures efficient signal transmission in WBAN as interference

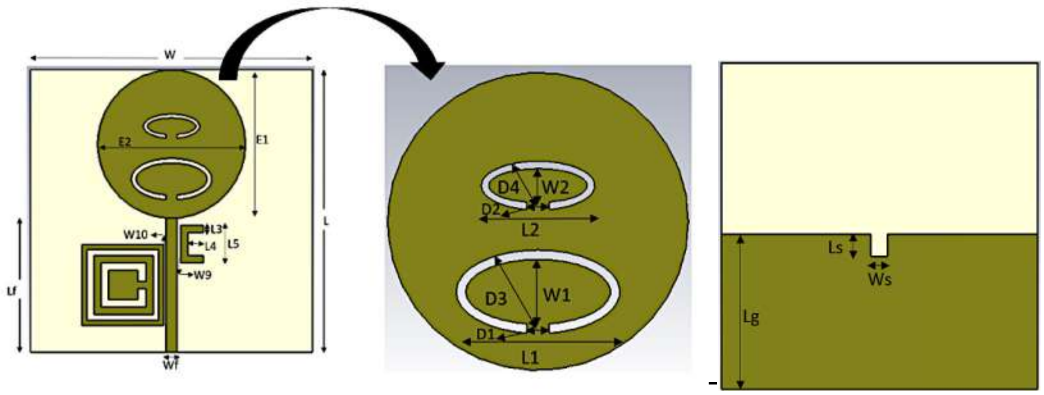

(a) (b)

Fig. 1 Proposed antenna design **a** Front view **b** Back view

with medical telemetry systems is rejected due to notched band.

- Internet of Things (IoT) and Sensor Networks—Can be use with IoT devices and wireless sensor networks, as it can avoid undesirable interference from existing wireless systems.

By incorporating band-notch characteristics, UWB antennas enhance system performance by eliminating disruptive signals while maintaining broadband operation.

The paper is organised in the following manner: Sect. 3 presents a summary of the design structure and the specific measurements. This section provides a thorough explanation of the procedure for achieving numerous band notches and explores the assessment of the design. Section 4 provides a concise discussion on the analysis of reflection coefficients in relation to different design topologies, variations in parameters, diverse substrate materials, surface current distribution, and antenna impedance. In Sect. 5, we give an analysis of the measured results, with a specific focus on aspects such as the reflection coefficient, radiation pattern, and gain. The next section serves as the conclusion of the paper.

3 Design and configuration

Figure 1 depicts the forward and posterior perspectives of the antenna. In order to obtain the Ultra-Wideband (UWB) spectrum, a patch with an elliptical shape is created on the upper surface of the substrate. The patch has a major axis length (E1) and a minor axis length (E2). At the same time, a partial ground plane is added to the underside of the substrate. The design is executed on a substrate made of FR4 epoxy material, which has a thickness of 0.8 mm. The substrate has dielectric constants of $\varepsilon r = 4.4$ and a loss tangent of 0.02. A slot measuring 2.5×1.5 mm^2 is incorporated into the partial ground plane to improve the impedance bandwidth

Table 1 The proposed penta-notch UWB antenna dimensions

Parameter	Value (mm)	Parameter	Value (mm)	Parameter	Value (mm)	Parameter	Value (mm)
L	38	W9	0.15	W7	0.5	D2	0.5
W	38	K1	2.22	W8	0.75	D3	4.67
W1	4.34	K2	2.3	G	1	D4	3.548
L1	8.9	W10	0.15	D	0.2	E1	9.95
L2	6.94	Wf	1.5	L3	1.58	E2	9.63
W2	2.678	Lf	18.08	L4	2.19	W3	11
D1	0.5	Lg	18	L5	6.42	W4	8
W5	4.5			Ls	1.5		

W, L Width and length of the overall antenna substrate, *Wf, Lf* Width and length of the feeding transmission line, *E1, E2* Circular patch dimensions, *L1, L2* Lengths related to the ring dimensions, *L3, L4, L5* Lengths defining various sections of the slot, *D1, D3* Diameters of the circular slots in the patch, *D2, D4* Diameters of the inner rings within the patch, *W1, W2* Widths of the rings, *Lg* Length of the ground plane, *Ls* Slot length in the ground plane, *Ws* Slot width in the ground plane, *W9, W10* Widths dimensions for specific feed-line,

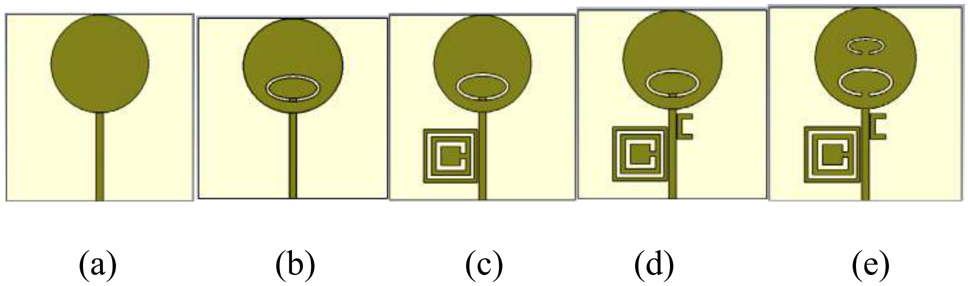

Fig. 2 Design procedure **a** Design 1 **b** Design 2 **c** Design 3 **d** Design 4 **e** Proposed design

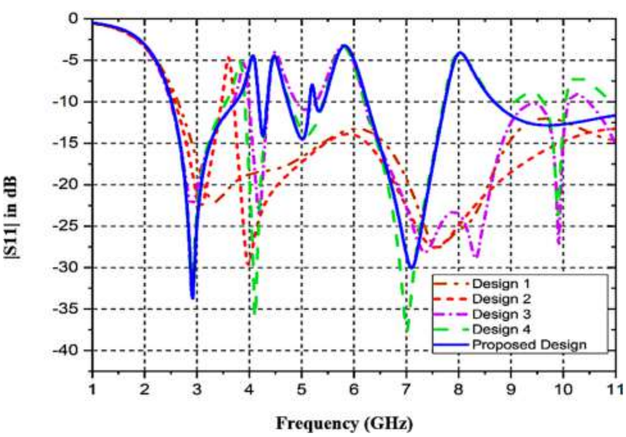

Fig. 3 Simulated graphs for return loss of Design1, Design2, Design3, Design 4 and proposed design

of the design. The enhanced bandwidth now covers the frequency range of 2.5–11 GHz. The radiating patch is connected to a 50-Ω micro strip line, which has a specific length (Lf) and width (W_f). Table 1 presents a thorough compilation of the optimised measurements for the suggested design.

The following stages clarify the procedures for creating notches at different frequencies. Figure 2(b) illustrates the second design, which involves carving an elliptical slot from the radiating patch to create a notch at the C-band (3.7–4.2 GHz). In order to achieve both frequencies at INSAT (4.5–4.7 GHz) and the higher WLAN band (5.725–5.825 GHz) simultaneously, a TVDS-EBG is built near the feed line, as shown in Fig. 2(c). In addition, a frequency gap within the range of 7.95–8.55 GHz is created using SIR, as depicted in Fig. 2d. In order to achieve a total of five notches, an additional elliptical slot is incorporated into the patch, as illustrated in Fig. 2(e), resulting in a notch at the lower WLAN band (5.15–5.35 GHz). Figure 3 exhibits the return loss graph for Design 1, Design 2, Design 3, Design 4, and the suggested design. The graph representing Design 1 shows an S11 value that remains below -10 dB across the frequency range of 2.5–GHz, thereby satisfying the criteria for Ultra-Wideband (UWB) specifications.

3.1 Techniques to create notches

The surface current in the selected notch bands is confined to specific regions of the spot by the process of etching elliptical slots and utilising Electromagnetic Band Gap (EBG) structures. Within this arrangement, five bands have been eradicated using diverse methods, which will be explained in detail below.

3.1.1 C-band and lower WLAN band rejection

In order to achieve certain frequencies in the C-band and the lower WLAN band, two Elliptical Split Ring Resonators (ESRR) are engraved onto the patch, as depicted in Fig. 2(a) and (e). The dimensions of the ESRR at the notch frequency are calculated using the calculations provided in reference [30].

$$\mathrm{Ci} = \frac{\mathrm{c}}{2 * \mathrm{fnotch}\sqrt{\varepsilon\mathrm{eff}}} = \pi(a+b)\left(1+3h/\left(10+\sqrt{4-3h_e}\right)\right) \tag{1}$$

$$h_e = (\mathrm{a}-\mathrm{b})^2/(\mathrm{a}+\mathrm{b})^2 \tag{2}$$

$$\epsilon\mathrm{eff} = \frac{\varepsilon\mathrm{r}+1}{2} + \frac{\frac{\varepsilon\mathrm{r}-1}{2}}{\sqrt{1+\frac{12h}{Wf}}} \tag{3}$$

Table 2 Calculated C-band and lower WLAN notched frequency due to ESRR

ESRR	Frequency (Simulated)	Frequency (calculated)	ϵeff	A (half of the major axis)	B (half of the minor axis)	Ci	h_e
Small (Lower WLAN)	5.25 GHz	5.13 GHz	3.33	a = L2/2 = 6.94/2 = 3.47 mm	b = w2/2 = 2.678/2 = 1.34 mm	16.03 mm	0.1958
Large (C-band)	3.91 GHz	3.84 GHz	3.33	a = L1/2 = 8.9/2 = 4.45 mm	(b = w1/2 = 4.34/2 = 2.17 mm)	21.40 mm	0.1186

Here, Ci denotes the inner circumference of the ESRR. It is expected to be around half of the guided wavelength at the notch frequency. The variable h denotes ellipticity which is the factor of half of the major and minor axis of the ESRR. The effective dielectric constant ε_{eff} is calculated using Eq. (3), where W_f denotes the width of the micro strip line, 'h' signifies the height of the substrate. Calculated notched frequency using the Eqs. (1–3) and dimensions of ESRRs are given in Table 2. Calculated frequencies are in close approximation to the simulated frequencies.

The ESRR, which is present in the lower portion of the patch and has the following characteristics: major axis length L1, minor axis length W1, ellipticity k1, and cut width D3, forms the notch at the C-band. The lower ESRR is the focus of the current distribution at 4.02 GHz, which effectively blocks radiation outside of this designated zone (described in the following section). The optimised value is 11.65 mm, resulting in a C-band notch, but the computed Ci value using the equations is 11.5 mm. The parametric analysis of the D1 parameter is shown in Fig. 4. Notch moves from 3.55 to 3.7 mm as D1 (gap between two edges of ESRR) grows. The ideal D1 value, which results in a notch with a frequency range of 3.7–4.12 GHz, is 0.5. A notch in the lower WLAN is formed by the ESRR with major axis length L2, minor axis length W2, ellipticity k_2, and cut width D4 in the upper portion of the radiating patch.

The C-band notch is created by the ESRR positioned in the lower part of the patch. The ESRR is defined by its major axis length (L1), minor axis length (W1), ellipticity (k_1), and cut width (D3). At a frequency of 4.02 GHz, the current is mainly focused in the lower ESRR, successfully preventing radiation from extending beyond this region (as explained in the subsequent section). The Ci value calculated using the calculations stated above is 16.03 mm, whereas the optimised value is 16.65 mm, guaranteeing the existence of a C-band notch.

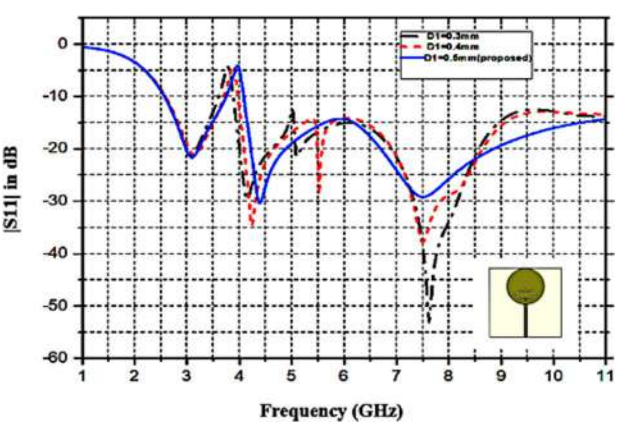

Fig. 4 Simulated graphs for return loss showing parametric variation of D1 parameter

Figure 4 illustrates the parametric analysis of the D1 parameter. As the magnitude of D1 (the distance between two edges of ESRR) grows, the notch moves from 3.55 to 3.7 mm. The most favourable selection for D1 is 0.5, leading to a notch spanning from 3.7 to 4.12 GHz. The top part of the radiating patch includes ESRR, which has a major axis length of L2, a minor axis length of W2, an ellipticity of k_2, and a cut width of D4. This configuration results in a notch at the lower WLAN.

Design-2, as seen in Fig. 2(a), features the initial ESRR carved near the feed point on the patch. This results in the creation of band stop characteristics that uniquely affect the C-band satellite downlink channel. As shown in the graph for design-2 in Fig. 4, the S11 value stays below − 10 dB between the frequencies of 3.7 GHz and 4.12 GHz. The middle frequency of the notch is 3.91 GHz. This confirms the existence of the initial notch in the C-band, whereas the remaining portion of the ultra-wideband (UWB) spectrum maintains consistent impedance characteristics.

3.1.2 INSAT and upper WLAN band rejection

EBGs represent a distinctive category of metamaterials characterized by their unique band gap property, a feature strategically employed in antenna design to eliminate undesired frequency bands. In this context, a specialized EBG structure known as the two via double slot (TVDS) type [23, 31, 32] is implemented in close proximity to the feed line to effectively reject signals from both the INSAT and upper WLAN bands. The revised antenna design, denoted as design-2, is illustrated in Fig. 2(c), while the geometric details of the EBG structure are presented in Fig. 5(a).

The EBG structure comprises an inner square patch with a side length of W5, a shorting via with a diameter of D, and specific dimensions for the outer slot (W6), inner patch width (W5), and the gap between the micro strip line and the EBG structure (W10). The TVDS-EBG structure, featuring a two via double slot configuration, is capable of generating dual notches due to the presence of two series resonant circuits within a single cell.

The equivalent circuit, depicted in Fig. 5(b), reveals the key components contributing to the dual resonance frequencies. Inductance (L1) arises from the current flow between the vias situated on the edge, the ground, and the via within the inner patch. Capacitance (C1) is established between the outer slot and inner patch, with a gap of W7. Together, C1 and L1 constitute the first resonant circuit. Additionally, the second resonant circuit is formed by capacitances C2, C3, and C4, along with inductance L2. Specifically, C2 is associated with the inner slot and inner patch, C4 is linked to the gap between adjacent EBG cells, and C3 is created due to the gap between the outer slot and inner patch.

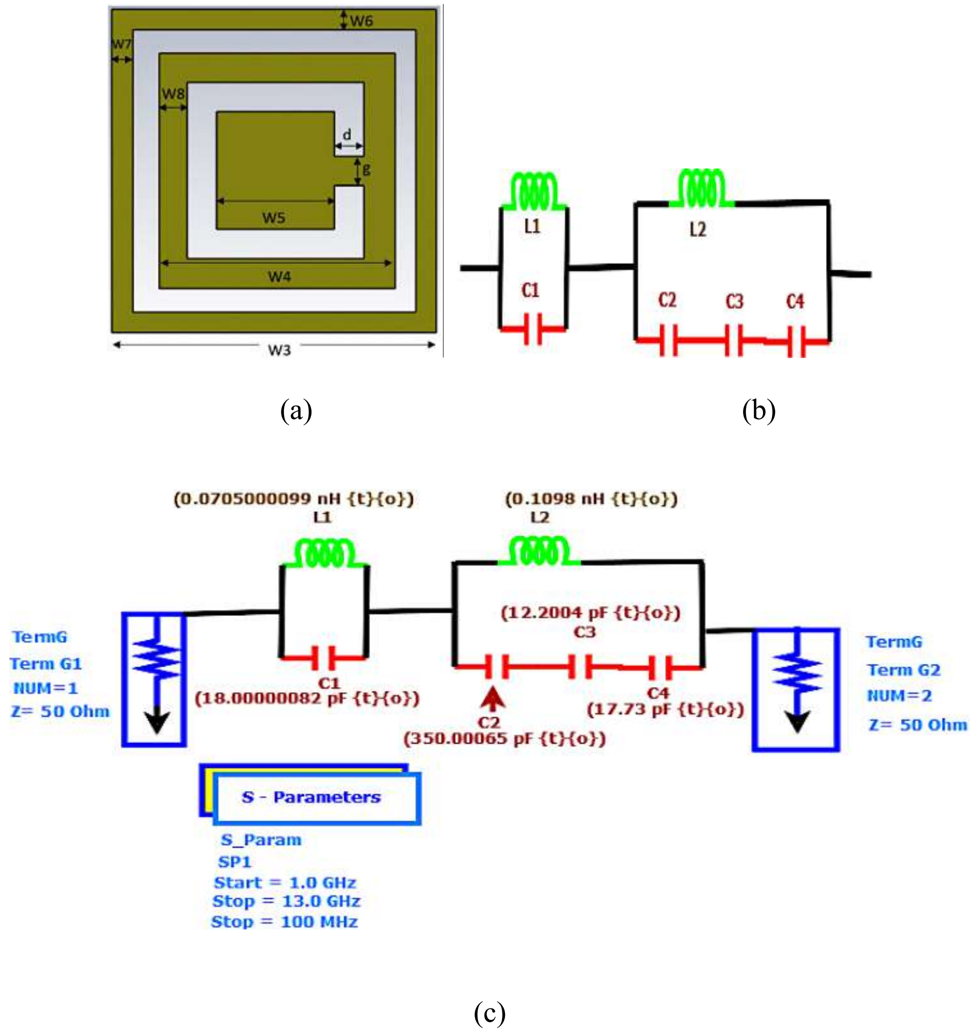

Fig. 5 **a** TVDS-EBG structure **b** Equivalent circuit of EBG **c** Equivalent circuit of EBG in ADS schematic environment

The TVDS-EBG structure and the corresponding unit cell's equivalent circuit diagram are depicted in Fig. 5, providing insight into the intricate interplay of components. The dual resonance frequencies of the TVDS-EBG structure can be determined using Eqs. (4–6).

$$Fc1 = \frac{1}{2 * \pi\sqrt{L1C1}} \tag{4}$$

$$Fc2 = \frac{1}{2\pi\sqrt{L2C_{eq}}} \tag{5}$$

Here,

$$\frac{1}{Ceq} = \frac{1}{C2} + \frac{1}{C3} + \frac{1}{C4} \tag{6}$$

The ADS Schematic environment was used to simulate the equivalent circuit of EBG, as shown in Fig. 5(c), in order to estimate the values of passive components (L1, C1, L2, C2, C3, and C4). The tuning feature in ADS was utilised to change different parameter values in order to match the simulated S11 curve. Tables 3 and 4 display the values of the simulated, measured, and comparable circuit notch frequencies.

We utilised the Ansys high-frequency simulator to do simulations utilising the Eigen mode solution in order to evaluate the band gap properties of TVDS-EBG. A unit cell

Table 3 Comparison of simulated

Notch Band	Notched frequency (GHz) (Simulated)	notched frequency (GHz) (Measured)	LC equivalent circuit frequency (GHz) (Calculated)	C1 (pf)	L1 (nH)
INSAT	4.53	4.5	4.48	0.18	0.07

Measured and LC equivalent lumped element notch frequency at 4.5 GHz

Table 4 Comparison of simulated

Notch Band	Notched frequency (GHz) (Simulated)	LC Equivalent Circuit frequency (GHz) (Measured)	Notched frequency (GHz) (Calculated)	C4 (pf)	C3 (pf)	L2 (nH)	C2 (pf)
Upper WLAN	5.84	5.68	5.9	17.83	12.2	0.11	350

Measured and LC equivalent lumped element notch frequency at 5.8 GHz

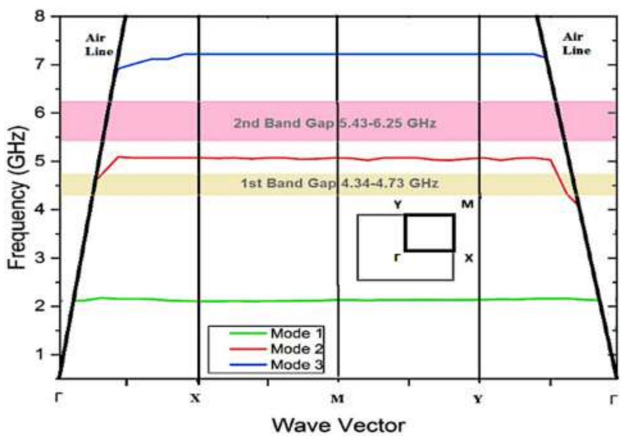

Fig. 6 Dispersion diagram for TVDS-EBG structure

was used to create a rectangular dispersion diagram based on the irreducible Brillouin zone, as shown in Fig. 6. The band gaps were identified by doing dispersion analysis on a single cell. To generate an infinite structure, periodic boundary conditions (PBC) were applied to the unit cell using the Eigen mode solver of HFSS. Figure 6 depicts the dispersion diagram for the unit cell, with the frequency represented on the vertical axis and the transverse wavenumbers kx and ky, which signify wave propagation vectors, displayed on the horizontal axis. The vectors included within the unit cell define the boundary region where waves can propagate, which is referred to as the irreducible Brillouin zone. The initial mode starts at a frequency of zero and gradually increases with the wave number, reaching its highest point at 4.73 GHz. The initial band gap arises between Mode 1 and Mode 2, covering a frequency range of 4.34–4.73 GHz. The subsequent band gap, located between Mode 2 and Mode 3, is visible at 5.43–6.25 GHz. The identified band gaps indicate the lack of surface waves in this frequency range.

The structure of the antenna, which includes the Electromagnetic Band Gap (EBG) structure, is shown in Fig. 2(c). Figure 3 displays the |S11| curve for design-3 to evaluate the influence of the selected EBG structure. The second and third notches are observed between the frequency range of 4.34–4.73 GHz, and between 5.43 GHz and 6.25 GHz, with centre frequencies at 4.53 GHz and 5.84 GHz, respectively. This leads to the formation of notches at the INSAT and upper WLAN frequency ranges, in addition to the initial notch.

3.1.3 ITU band (7.95 to 8.55 GHz) rejection

In order to reject the ITU band, a step-impedance-resonator (SIR) is added on the right side of the microstrip feed at a gap of 'w9'. Antenna geometry with SIR is shown in Fig. 2(d). SIR act as a band-pass filter and a non-uniform transmission line resonator. Coupling in feed line and resonator is maximum with minimum gap.

Equations (7 and 8) gives the relation between SIR dimensions and frequency

$$f_{s1} = \pi f_o / \left(2 \tan^{-1} \sqrt{k}\right) \tag{7}$$

where k is the impedance ratio.

$$\mathrm{L5} = \tan^{-1} \sqrt{k} \tag{8}$$

Here, f0 is the centre resonance frequency (8.25 GHz) of ITU band and fs1 is the first spurious resonance frequency. Design 4 curve in Fig. 4 represents the fourth notch at 7.73 GHz–8.69 GHz having a centre frequency of 8.21 GHz in addition to three notches. Finally, Design-4 is altered by etching the second ESRR in the patch as shown in Fig. 2(e) which is the proposed structure. It causes the band suppression at lower WLAN band with frequency ranging from 5.15 to 5.26 GHz. In this way, the proposed design is able to produce a penta notch in UWB range. Furthermore, to confirm the characteristics of ESRR and EBG antenna plot of relative permittivity and permeability are represented in Fig. 7. Figure 7(a) shows the negative permittivity (real) at the frequencies of of 3.9, 4.53, 5.25, 5.84, and 8.25 GHz. The imaginary values of effective permittivity are positive, which confirms the criteria for metamaterial behaviour. The effective permeability (real) values are lying near to zero at each resonance, with an amplitude of 0.038, 0.049, 0.716, 0.543, and 0.12, respectively at the notched frequencies.

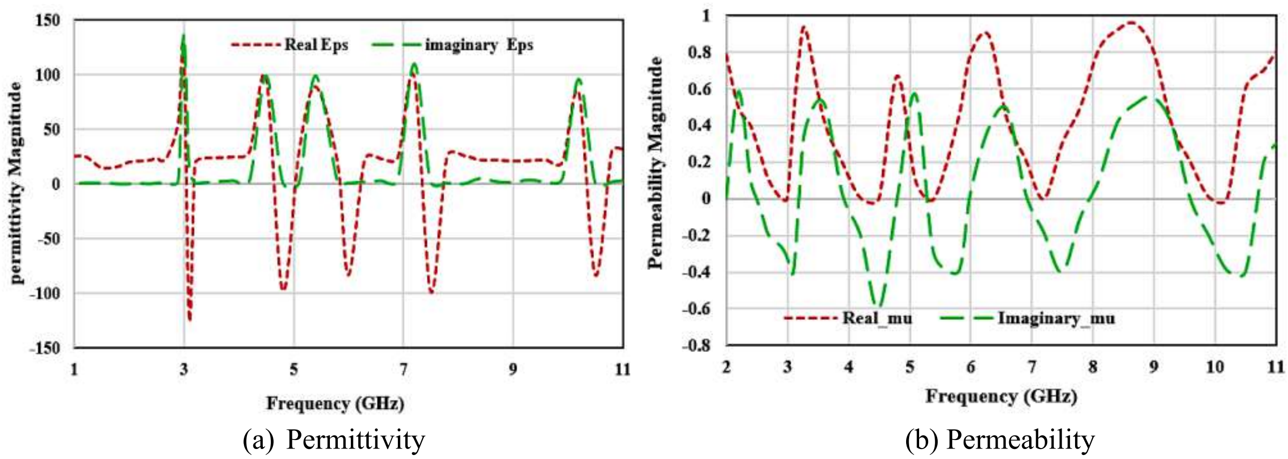

Fig. 7 Plot for **a** Permittivity and **b** Permeability of antenna at notched frequency

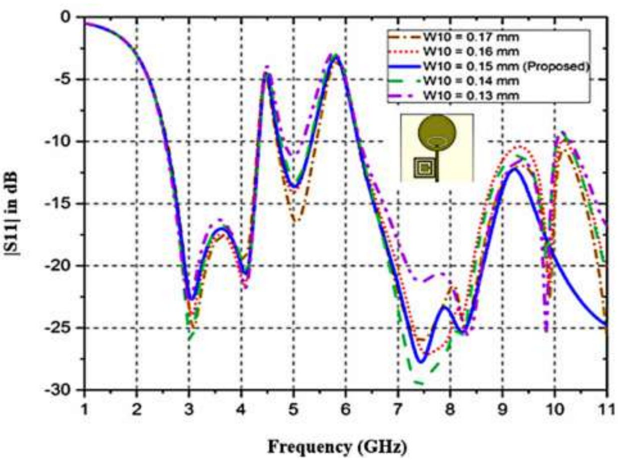

Fig. 8 Return loss variations of EBG structure with varying gap W10 with feed line

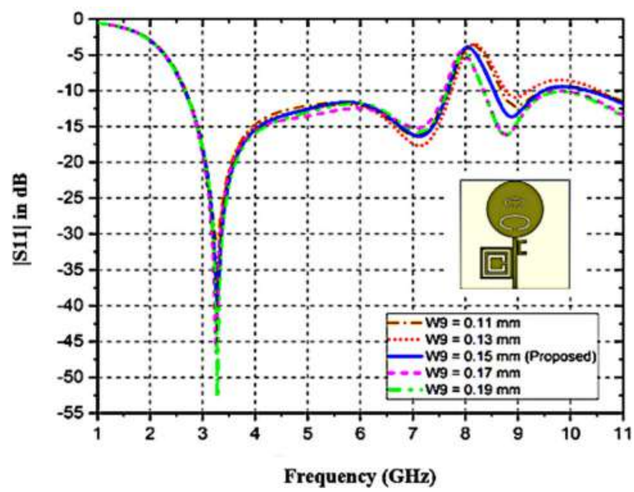

Fig. 9 Return loss variations of SIR structure with varying gap w9 with feed line

4 Results and discussion

This part delves into the parametric analysis of the antenna, specifically investigating the distribution of surface currents and the impedance curve of the proposed design. An exhaustive study is performed to examine the discrepancy between the EBG structure and the feed line 'W10.' Fig. 8 displays the plot of the reflection coefficient for different values of 'W10'. It shows that as the gap increases from 0.13 to 0.17 mm, both the bandwidth and depth of the notches decrease. This phenomenon is caused by the reduced mutual interaction between the electromagnetic bandgap (EBG) and the feed line. A gap of 0.15 mm produces notches at the specified frequencies for INSAT (4.5–4.7 GHz) and the higher WLAN band (5.725–5.825 GHz), which range from 4.34 to 4.73 GHz and from 5.43 to 6.25 GHz, respectively.

In addition, a vital parametric analysis is conducted to assess the gap between the SIR structure and the feed line labelled 'W9'. Figure 9 illustrates the plot of the reflection coefficient as it varies with 'W9'. By widening the distance from 0.11 to 0.19 mm, the depth of notches and bandwidth decrease as a result of the diminished mutual coupling between the feed line and SIR. A gap of 0.15 mm achieves the desired notch at the ITU band (7.95–8.55 GHz), making it the chosen value for the design.

An analysis was performed on the surface current distribution of the radiating patch, the Electromagnetic Band Gap (EBG) structure, and the SIR to understand the antenna's behaviour. Figure 10 depicts the plot showing the distribution of current at notched bands. At a frequency of 3.91 GHz, the electric current mostly focuses on the lower Electrically Small Radiating Region (ESRR), preventing

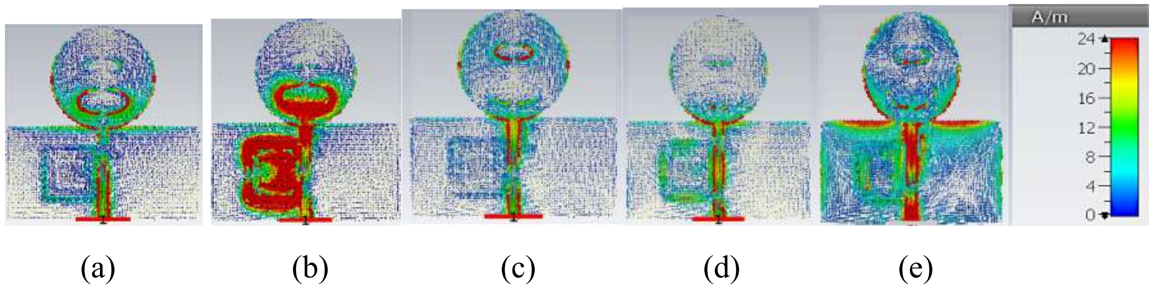

Fig. 10 Surface current distribution of proposed design at **a** 4.02 GHz **b** 4.54 GHz **c** 5.22 GHz **d** 5.9 GHz **e** 8.08 GHz

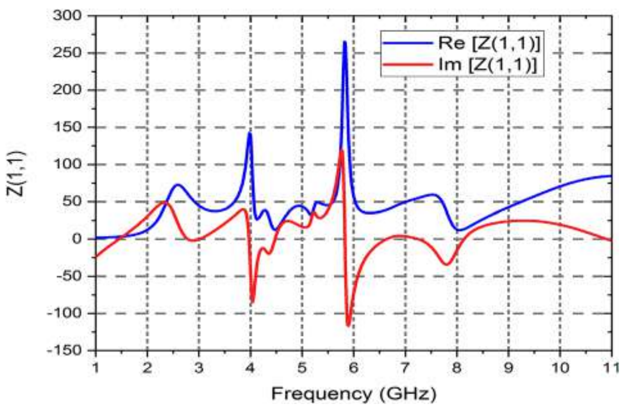

Fig. 11 Input impedance of proposed antenna

Fig. 12 Fabricated prototype **a** Front view **b** Back view

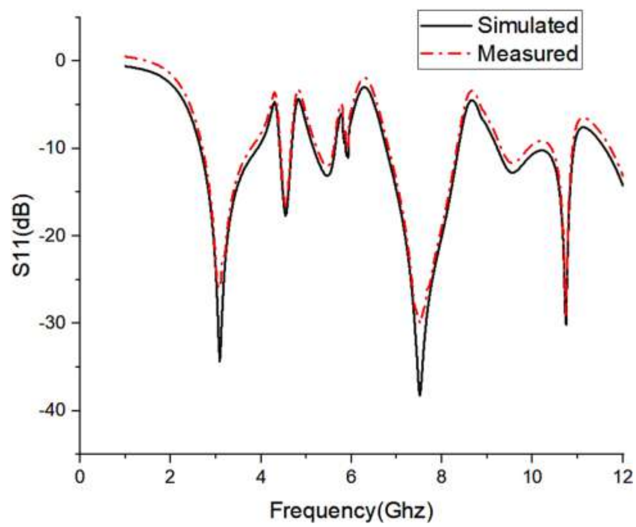

Fig. 13 Simulated and measured reflection coefficient

radiation beyond the borders of the ESRR (Fig. 9a). As the frequency increases, the current moves towards the Electromagnetic Band Gap (EBG) structure at 4.53 GHz and 5.84 GHz, as seen in Figs. 9b and d. This leads to reduced radiation at these frequencies. Figure 9(c) demonstrates that at a frequency of 5.20 GHz, the focal point of the current changes towards the upper ESRR. Similarly, at a frequency of 8.21 GHz, the current density surrounds the SIR, as depicted in Fig. 9(e). Significantly, current amplifies at specific frequencies at band-notched elements, indicating increased energy storage around these components rather than emission into the surrounding environment. This highlights the band rejection properties of the suggested design over five frequency bands. The impedance curve displayed in Fig. 11 demonstrates that inside the Ultra-Wideband (UWB) range, the resistance remains close to 50 ohms, while the reactance almost reaches 0 ohms, except at the notches.

The resistance is significantly increased in the first notch (3.76–4.10 GHz) and the fourth notch (5.5–6.32 GHz), measuring at 140 ohms and 270 ohms, respectively. In addition, the reactance is negative, similar to that of a parallel RLC circuit. Conversely, the resistance measures less than 50 ohms at the second notch (4.42–4.74 GHz), the third notch (5.17 to 5.27 GHz), and the fifth notch (7.76 to 8.88 GHz). In such instances, the reactance exhibits a positive value, mirroring the characteristics of a series resonance circuit.

Figure 12 portrays the constructed design from both the front and back views. The return loss graph was evaluated using a vector network analyser, and the radiation characteristics were computed in an anechoic chamber. Figure 13 illustrates the plotted comparison of the simulated and measured graphs for the reflection coefficient of the suggested design. Notably, the S11 value surpasses − 10 dB within five notched bands and remains below − 10 dB for all other

Fig. 14 Comparison of measured and simulated radiation

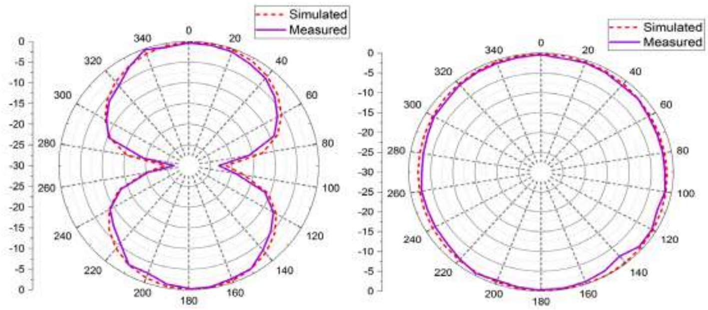

(a) 2.92 GHz (E- plane) (b) 2.92 GHz (H-plane)

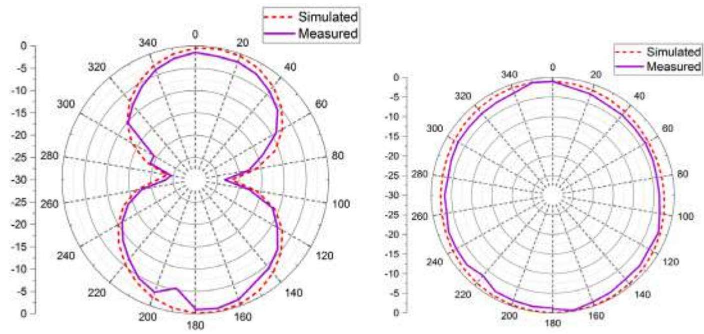

(c) 4.26 GHz (E- plane) (d) 4.26 GHz (H-Plane)

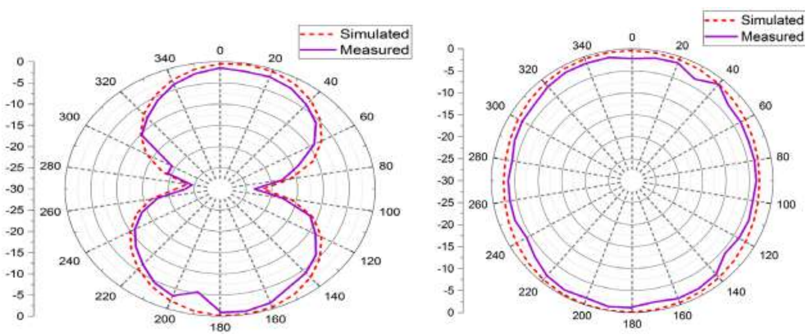

(e) 5 GHz (E-plane) (f) 5GHz (H-plane)

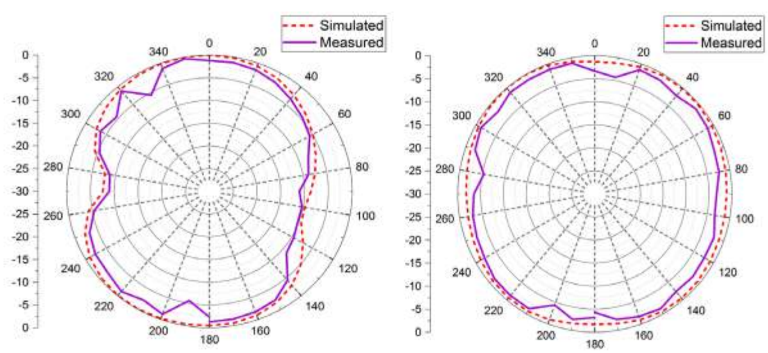

(g) 7.12 GHz (E-plane) (h) 7.12 GHz (H-plane)

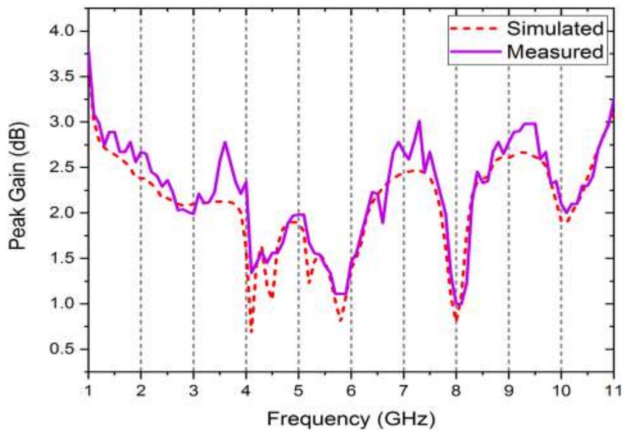

Fig. 15 Simulated and measured peak gain comparison

frequencies spanning from 2.5 to 11 GHz. The correlation between the simulated and measured S11 values is typically acceptable, however there is a tiny discrepancy towards lower frequencies, which could perhaps be attributed to variations in soldering temperature and tolerances [25]. There are several factors that leads to variation in antenna impedance while measurement at lower frequencies; lower frequencies have larger dimension making antenna impedance more sensitive to the manufacturing inaccuracies like etching errors and soldering of connector. Permittivity and loss tangent of substrate varies more at lower frequencies. In addition to this, parasitic effect of measurement set up and coupling to surrounding conditions is higher at the lower frequencies.

The antenna demonstrates outstanding performance throughout the intended ultra-wideband (UWB) frequency range, with specific frequency bands that are aligned with five communication standards. This attribute makes the antenna highly suitable for UWB communication without generating interference with other narrow-band standards.

The radiation pattern plots for the proposed design are assessed at frequencies of 2.92 GHz, 4.26 GHz, 5 GHz, and 7.12 GHz, measured in both E-planes and H-planes. The comparisons between the observed patterns and the simulated patterns are shown in Fig. 14(a–d) for their corresponding frequencies. An omnidirectional radiation pattern is detected in the H-plane, whereas a dipole-like radiation pattern is observable in the E-plane for both the measured and simulated equivalents. The measured and computed radiation patterns closely align, with the exception of a minor difference at 7.12 GHz. The discrepancy may be ascribed to the amplified dielectric dissipation in the FR4 substrate at elevated frequencies.

Figure 15 demonstrates the correlation between the observed and simulated peak gains, showing a maximum gain of 3 dB at 9.5 GHz and 2.5 dB at 9.3 GHz, respectively. The peak gain exhibits a decrease at frequencies of 3.91 GHz, 4.53 GHz, 5.2 GHz, 5.84 GHz, and 8.21 GHz, showing the existence of a quintuple notch generated by

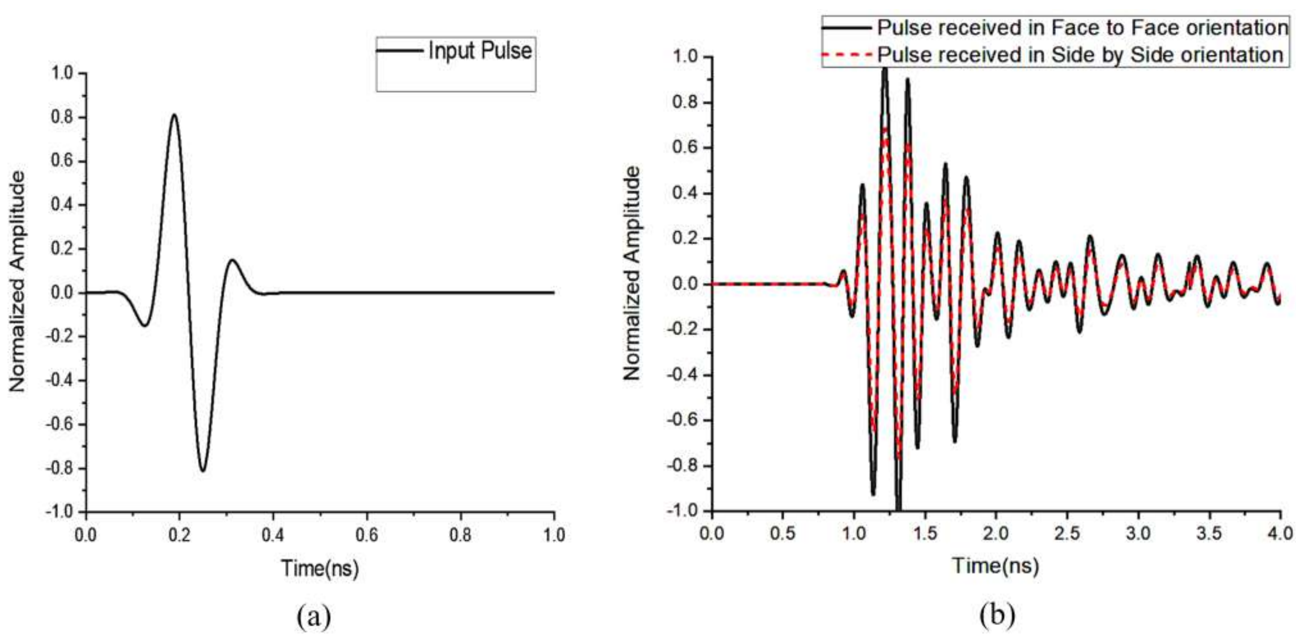

Fig. 16 Transient time domain analysis of proposed notched-band antenna **a** Input pulse **b** Received pulses

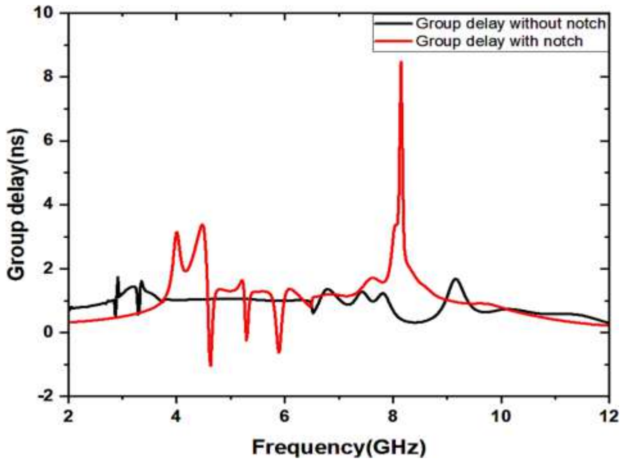

Fig. 17 Group delay without and with notch bands

the suggested antenna. However, the maximum increase in signal strength stays above 2 dB for the remaining frequencies within the Ultra-Wideband (UWB) range.

The transient solution type feature was used to evaluate the pulse handling capability of the proposed design in time domain analysis. A waveform characterised by a sudden change in signal served as the input, and the subsequent output was observed. Figure 16 demonstrates that the presence of notches at specific frequencies (3.91 GHz, 4.53 GHz, 5.2 GHz, 5.84 GHz, and 8.21 GHz) results in amplified ringing and distortion of pulses. Nevertheless, the entire duration of the pulse remains limited to the 2 ns interval, thus establishing a data rate of 500 megahertz.

Figure 17 illustrates the group delay of the suggested system. Group delay is the negative-slope of the transmission phase angle with respect to frequency.

$$\text{Group delay } = -\frac{1}{2\pi}\left(\frac{d\text{Ø}}{df}\right) \tag{9}$$

where Ø is the phase angle and f is the frequency.

While measuring the |S11| through VNA, the phase angle is also received at the different frequency points. Then the group delay formula is used to evaluate the values plotted in Fig. 16.

The group delay remains consistently below 2 ns over the whole ultra-wide bandwidth for the antenna without any notches. Nevertheless, within the notch bands, there is a conspicuous augmentation in group delay, which signifies the presence of distortion at these particular frequencies. Table 5 presents a comparison between the proposed design and similar antennas that have been reported in the past. The suggested antenna has superior performance in terms of both bandwidth and Bandwidth to dimension ratio (BDR) than the earlier similar five-notched band UWB antennas. BDR is the important parameter of a UWB antenna. The higher the BDR, the more compact is the antenna, and the wider the operating bandwidth. BDR is calculated as:

$$\text{BDR} = \text{Fractional Bandwidth}/(\mu\lambda\text{length} \times \mu\lambda\text{width}) \tag{10}$$

where, ƛlength and ƛwidth are the antenna length and width respectively in terms of wavelength.

Reference [34] mentioned in Table 4 has bandwidth little higher than that of the proposed one but it yields lower value of BDR than that of the proposed geometry. Also, Reference [35] shows the geometry having BDR little higher than that of the proposed geometry but its measured gain value is much lower than that of the proposed one.

Table 5 Comparison of the proposed antenna with existing antennas

References	Bandwidth (GHz)	Number of notches	Dimension (mm^3)	Notched frequency band (GHz)	Peak gain (dB)	BDR (%)
[33]	2.2–11	5	80 × 80 × 0.508 (= 3251.2)	(1.85–2.49), (2.91–3.49), (5.65–6.25), (7.19–8.78)	–	0.96
[34]	2.86–13.3	5	36 × 38 × 1.6 (= 2188.8)	(3.45–4), (5.15–5.9), (6.77–8), (8.3–9.1), (9.3–10.6)	4.51	2.5
[35]	3.05–10.6	5	31 × 25 × 1.6 (= 1240)	(3.4–3.8), (5.1–5.35), (5.6–6), (7.15–7.65), (8.05–8.65)	1.62	3.45
[36]	2.9–10.5	5	31.3 × 34.9 × 1.6 (= 1747.7)	(2.4–2.9), (3.6–4.3), (5.3–5.7), (6.4–6.7), (7.8–8.6)	3.1	2.7
Proposed work	2.5–11	5	38 × 38 × .8 (= 1155.2)	(3.7–4.12), (4.34–4.73), (5.43–6.25), (7.73–8.69), (5.15–5.26)	3.25	3.14

5 Conclusions

In this article, a five-band-notched UWB antenna is designed. Metamaterials are integrated to reject the desired frequency bands, and their effects are analyzed using a mathematical model and surface current distribution. The five rejected bands are the satellite downlink C-band (3.7–4.2 GHz), the lower WLAN band (5.15–5.35 GHz), the upper WLAN band (5.725–5.825 GHz), the INSAT band (4.5–4.7 GHz), and the ITU band (7.95–8.55 GHz). The performance of the notched bands is evaluated through simulated and measured reflection coefficients. In the E-plane, the antenna exhibits dipole-like radiation characteristics, while in the H-plane, it maintains omnidirectional radiation characteristics with a gain of 3 dB. The wide impedance bandwidth of 8.5 GHz and stable radiation performance make the proposed antenna a suitable candidate for UWB systems.

Acknowledgements The authors gratefully acknowledge Universiti Teknikal Malaysia Melaka (UTeM) and the Malaysian Ministry of Higher Education (MOHE) for their support in this research.

Author contributions Sapna Arora was responsible for conceptualization, methodology, data curation, and manuscript writing. Sharad Sharma supervised the study, validated the methodology, and reviewed the manuscript. Rohit Anand conducted formal analysis, validated the data, and contributed to manuscript editing. Anupma Gupta was involved in investigation, experimental work, and data interpretation. Ramesh Kumar provided resources and managed the project. Ahmed Jamal Abdullah Al-Gburi contributed to manuscript refinement, theoretical modeling, result interpretation, critical revision, and project administration. All authors have read and approved the final manuscript.

Data availability No datasets were generated or analysed during the current study.

Declarations

Conflict of interest The authors declare no conflict of interest.

References

1. Bekasiewicz, A., & Koziel, S. (2016). Compact UWB monopole antenna for internet of things applications. *Electronics Letters, 52*(7), 492–494.
2. Al-Gburi, A. J. A., et al. (2022). Super compact UWB monopole antenna for small IoT devices. *Computers, Materials and Continua, 73*(2), 2785–2799. https://doi.org/10.32604/cmc.2022.028074
3. Kumar, O. P., Kumar, P., Ali, T., Kumar, P., & Subhash, B. K. (2023). A quadruple notch uwb antenna with decagonal radiator and Sierpinski square fractal slots. *Journal of Sensor and Actuator Networks, 12*(2), 24.
4. Al-Gburi, A. J. A., Ibrahim, I., Zakaria, Z., et al. (2021). High gain of UWB CPW-fed Mercedes-shaped printed monopole antennas for UWB applications. *Prz Elektrotechniczny, 5*, 70–73.
5. Singh, I., Rehni, A. K., Kalra, R., Joshi, G., Kumar, M., & Aboul-Enein, H. Y. (2007). Ion exchange resins: Drug delivery and therapeutic applications. *Fabad Journal of Pharmaceutical Sciences, 32*(2), 91.
6. Kumar, G., & Kumar, R. (2019). A survey on planar ultra-wideband antennas with band notch characteristics: Principle, design, and applications. *AEU-International Journal of Electronics and Communications, 109*, 76–98.
7. Federal Communications Commission. Revision of part 15 of the commission's rules regarding ultra-wideband transmission systems. *First Report and Order, FCC 02-48,* 2022.
8. Dilruba Geyikoglu, M. (2023). A novel UWB flexible antenna with dual notch bands for wearable biomedical devices. *Analog Integrated Circuits and Signal Processing, 114*, 439–450. https://doi.org/10.1007/s10470-023-02146-y
9. Ibrahim, I. M., Al-Gburi, A. J. A., Zakaria, Z. O., & Bakar, H. A. (2018). Parametric study of modified U-shaped split ring resonator structure dimension at ultra-wide-band monopole antenna. *Journal of Telecommunication Electronic and Computer Engineering (JTEC), 10*(2–5), 53–57.
10. Yadav, S., Gautam, A. K., & Kanaujia, B. K. (2017). Design of dual band-notched lamp-shaped antenna with UWB characteristics. *International Journal of Microwave and Wireless Technologies, 9*(2), 395.
11. Kundu, S., & Chatterjee, A. (2021). Sharp triple-notched ultra wideband antenna with gain augmentation using FSS for ground penetrating radar. *Wireless Personal Communications, 117*(2), 1399–1418.
12. Chao, Z., Zitong, Z., Pei, X., Jie, Y., Zhu, L., & Gaosheng, L. (2022). A miniaturized microstrip antenna with tunable double band-notched characteristics for UWB applications. *Scientific Reports, 12*(1), 19703.
13. Al-Gburi, A. J., Ibrahim, I. M., & Zakaria, Z. (2017). Band-notch effect of U-shaped split ring resonator structure at ultra wide-band monopole antenna. *International Journal of Applied Engineering Research., 12*(15), 4782–4789.
14. Arora, S., Sharma, S., Anand, R., & Shrivastva, G. (2023). Miniaturized pentagon-shaped planar monopole antenna for ultra-wideband applications. *Progress In Electromagnetics Research C, 133*, 195–208.
15. Chen, Xu., Xu, F., & Tan, Xu. (2017). Design of a compact UWB antenna with triple notched bands using nonuniform width slots. *Journal of Sensors, 2017*, 1–9. https://doi.org/10.1155/2017/7673168
16. Lakrit, S., Das, S., Ghosh, S., & Madhav, B. T. P. (2020). Compact UWB flexible elliptical CPW-fed antenna with triple notch bands for wireless communications. *International Journal of RF and Microwave Computer-Aided Engineering, 30*(7), e22201.
17. Ghimire, J., & Choi, D. Y. (2019). Design of a compact ultrawideband U-shaped slot etched on a circular patch antenna with notch band characteristics for ultrawideband applications. *International Journal of Antennas and Propagation, 2019*, 8090936.
18. Emadian, S. R., & Ahmadi-Shokouh, J. (2018). Study on frequency and time domain properties of novel triple band notched UWB antenna in indoor propagation channel. *International Journal of RF and Microwave Computer-Aided Engineering, 28*(9), e21428.
19. Peddakrishna, S., & Khan, T. (2018). Design of UWB monopole antenna with dual notched band characteristics by using π-shaped slot and EBG resonator. *AEU-International Journal of Electronics and Communications, 96*, 107–112.
20. Sharma, A., Singh, H., Gupta, A., et al. (2024). Development and evaluation of wideband negative response in ultra-thin polygon metamaterial. *European Physical Journal B: Condensed Matter and Complex Systems, 97*, 61. https://doi.org/10.1140/epjb/s10051-024-00692-6

21. Abdullah Al-Gburi, A. J., Ibrahim, I., & Zakaria, Z. (2020). Gain enhancement for whole ultra-wideband frequencies of a microstrip patch antenna. *Journal of Computational and Theoretical Nanoscience, 17*(2), 1469–1473. https://doi.org/10.1166/jctn.2020.8827
22. Peng, L., & Ruan, C. L. (2011). UWB band-notched monopole antenna design using electromagnetic-bandgap structures. *IEEE Transactions on Microwave Theory and Techniques, 59*(4), 1074–1081.
23. Reddy, M. H., Sheela, D., Sharma, A., et al. (2021). A novel microstrip antenna loaded with EBG and ELC for bandwidth enhancement. *Analog Integrated Circuits and Signal Processing, 109*, 115–126. https://doi.org/10.1007/s10470-021-01935-7
24. Jaglan, N., Kanaujia, B. K., Gupta, S. D., & Srivastava, S. (2017). Design and development of an efficient EBG structures based band notched UWB circular monopole antenna. *Wireless Personal Communications, 96*(4), 5757–5783.
25. Liu, H., & Xu, Z. (2013). Design of UWB monopole antenna with dual notched bands using one modified electromagnetic-bandgap structure. *The Scientific World Journal, 2013*, 917965.
26. Chen, Z., Zhou, W., & Hong, J. (2021). A miniaturized MIMO antenna with triple band-notched characteristics for UWB applications. *IEEE access, 9*, 63646–63655.
27. Al-Gburi, A. J. A., Ibrahim, I. M., Zakaria, Z., & Khaleel, A. D. (2019). Bandwidth and gain enhancement of ultra-wideband monopole antenna using MEBG structure. *ARPN Journal of Engineering and Applied Sciences, Article, 14*(10), 3390–3393. https://doi.org/10.36478/JEASCI.2019.3390.3393
28. Sanmugasundaram, R., Natarajan, S., & Rajkumar, R. (2020). Ultrawideband notch antenna with EBG structures for WiMAX and satellite application. *ProgressIn Electromagnetics Research, 91*, 25–32.
29. Choudhary, H., Singh, T., Arif Ali, K., Vats, A., Singh, P. K., Phalswal, D. R., & Gahlaut, V. (2016). Design and analysis of triple band-notched micro-strip UWB antenna. *Cogent Engineering, 3*(1), 1249603.
30. Bhavarthe, P. P., Rathod, S. S., & Reddy, K. T. V. (2018). A compact dual band gap electromagnetic band gap structure. *IEEE Transactions on Antennas and Propagation, 67*(1), 596–600.
31. Xiao, J. K., Ma, S. W., & Li, Y. (2007). A compact microstrip stepped-impedance resonator and filter. *Microwave Journal, 50*(2), 116.
32. Dahiya, A., Anand, R., Sindhwani, N., & Kumar, D. (2021). A novel multi-band high-gain slotted fractal antenna using various substrates for X-band and Ku-band applications. *MAPAN*, 1–9.
33. Liu, J. J., Esselle, K. P., Hay, S. G., & Zhong, S. S. (2013). Planar ultra-wideband antenna with five notched stop bands. *Electronics Letters, 49*(9), 579–580.
34. Mewara, H. S., Deegwal, J. K., & Sharma, M. M. (2018). A slot resonators based quintuple band-notched Y-shaped planar monopole ultra-wideband antenna. *AEU-International Journal of Electronics and Communications, 83*, 470–478.
35. Islam, M. M., Islam, M. T., Samsuzzaman, M., & Faruque, M. R. I. (2015). Five band-notched ultra wide band (UWB) antenna loaded with C-shaped slots. *Microwave and Optical Technology Letters, 57*(6), 1470–1475.
36. Modak, S., Khan, T., & Laskar, R. H. (2020). Penta-notched UWB monopole antenna using EBG structures and fork-shaped slots. *Radio Science, 55*(9), 1–11.

Sapna Arora received her B.Tech degree in electronics and communication engineering from the Kurukshetra University, Kurukshetra, Haryana, India, in 2006. She has done her M.Tech degree in electronics & communication engineering from MDU University, Rohtak Haryana, India, in 2010. She is pursuing her PhD at MMU(DU), Ambala India. Her research interests include antenna designing, signal processing, and optical communication. She is a member of IEEE. She has published number of papers in reputed journals.

Sharad Sharma received his B.Tech in Electronics Engineering from Nagpur University, Nagpur, India in 1998 and M.Tech in Electronics and Communication Engineering from Thapar Institute of Engineering and Technology, Patiala, India in 2004. He has a teaching experience of more than 25 years. He has conducted many workshops on Soft Computing and its applications in engineering, Wireless Networks, Simulators etc. He has a keen interest in teaching and implementing the latest techniques related to wireless and mobile communications. He has opened up a student chapter of IEEE as Branch Counsellor. He has published 25 SCI/SCOPUS indexed research papers, 2 Books and 17 Book Chapters with international publishers. He has also published 4 patents. Presently, he is working as Professor and Head-Electronics and Communication Engineering Department MMEC, MMDU, Mullana, INDIA. His research interests are Internet of Things, Soft Computing, routing protocol design, performance evaluation and optimization for wireless mesh networks using nature inspired computing.

Rohit Anand is currently working as an Assistant Professor (Group-A Gazetted Officer) in the Department of Electronics and Communication Engineering at G. B. Pant DSEU Okhla-1 Campus (formerly G. B. Pant Engineering College), Government of NCT of Delhi, New Delhi, India. He has teaching experience of more than 21 years including UG and PG Courses. He is a Life Member of Indian Society for Technical Education (ISTE) and also a member of IEEE. He has published 14 book chapters in reputed books (under the Publishers like Springer, Wiley, IGI Global, Taylor and Francis, InTech) and 19 research papers in SCI/

Scopus Indexed Journals. He is the Editor of 3 reputed Edited Books. He has chaired Special Session in 16 International Conferences and presented more than 26 Research Papers in various National and International Conferences. He has also got 3 Patents (1 Published and 2 Granted). He has got Best Paper Presentation Award 2 times in an International Conference. He has received 2 Medals (1 Gold and 1 Silver) in NPTEL Online Certification Courses conducted by MHRD, Govt. of India. He has guided 12 Students in M.Tech. He has got 2nd Position in State Level Competition on National Science Day. His areas of research and interest include Electromagnetic Field Theory, Antenna Theory and Design, Optimization, Wireless Communication, Image Processing, Optical fibre Communication, IoT etc.

Anupma Gupta received B.E. degree in Electronics and Communication Engineering from Guru Jambheshwar University, Haryana, India in 2006 and M. Tech degree from Maharishi Markandeshwar University, Haryana, India in 2010. She completed his Ph.D. degree from the Department of Electronics Engineering, Thapar Institute of Engineering and Technology, Punjab, India in 2021. She is currently working as Assistant Professor-Chitkara University, Punjab, India. Her research interest includes computational Electromagnetics, reconfigurable antennas, novel electromagnetic materials, dielectric resonator antennas, wideband/super wide band antennas, wideband/dual band/triple band microstrip antennas for wireless communication, smart and MIMO antennas systems, antennas for healthcare, RF MEMS planar antenna, and IoT. She has published more than 50 research papers and granted with 13 patents. She is also reviewer of various reputed journals.

Dr. Ramesh Kumar received the B.E. In Electronics Instrumentation Control Engineering from the University of Rajasthan, Jaipur in 2007 and the M.Tech. Degrees in Instrumentation Control from Dr. B R Ambedkar National Institute of Technology Jalandhar, in 2009. And Ph.D. in Instrumentation from Dr. B R Ambedkar National Institute of Technology Jalandhar, in 2019. From 2014 to 2019 he was a Research Scholar with the Dr. B R Ambedkar National Institute of Technology Jalandhar under the Signal Processing Laboratory. He authorizes two books and more than 30 in SCI/Scopus/conference articles. He has received two MHRD CRS grant RD projects from Govt. of India (Mint). His research interests include biomedical instrumentation and tomography application in medicine and industrial settings. Currently working on many applications like cube set, fuel cell technology, renewable Energy sector, etc., and holds 8 patents.

Ahmed Jamal Abdullah Al-Gburi (Senior Member, IEEE) received his M.Eng. and Ph.D. degrees in electronics and computer engineering (telecommunication systems) from Universiti Teknikal Malaysia Melaka (UTeM), Malaysia, in 2017 and 2021, respectively. From December 2021 to March 2023, he was a Postdoctoral Fellow with the Microwave Research Group (MRG) at UTeM. He is currently a Senior Lecturer with the Faculty of Electrical and Electronic Engineering Technology (FTKEE) at UTeM. He has authored and co-authored numerous papers in journals and conference proceedings. His research interests include microwave sensors, metasurfaces, UWB antennas, array antennas, and miniaturized antennas for UWB and 5G applications. He is a member of the Board of Engineers Malaysia (BEM) and the International Association of Engineers (IAENG). He has received the Best Paper Award from the IEEE community and has earned several gold, silver, and bronze medals in international and local competitions. In 2023 and 2024, he was recognized as one of the top 2% of scientists worldwide by Stanford University, as published by Elsevier.